IEEE Photonics Journal
An IEEE Photonics Society Publication

Open Access

# Light Extraction Efficiency of GaN-Based Micro-Scale Light-Emitting Diodes Investigated Using Finite-Difference Time-Domain Simulation

Volume 12, Number 2, April 2020

Han-Youl Ryu
Jeongsang Pyo
Hyun Yeol Ryu

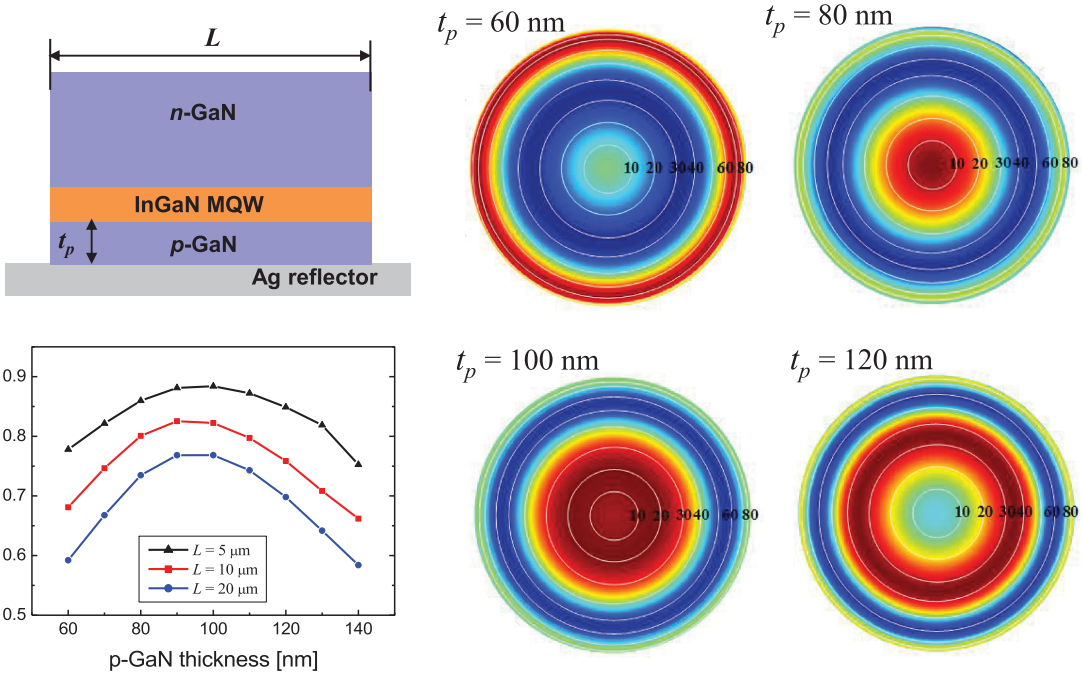


DOI: 10.1109/JPHOT.2020.2977401

# Light Extraction Efficiency of GaN-Based Micro-Scale Light-Emitting Diodes Investigated Using Finite-Difference Time-Domain Simulation

**Han-Youl Ryu, Jeongsang Pyo, and Hyun Yeol Ryu**

Department of Physics, Inha University, Incheon 22212, South Korea

*DOI:10.1109/JPHOT.2020.2977401*


Manuscript received February 21, 2020; accepted February 25, 2020. Date of publication March 2, 2020; date of current version March 26, 2020. This work was supported in part by the Basic Science Research Program through the National Research Foundation (NRF) of Korea funded by the Ministry of Education (2016R1D1A1B03932092), in part by the Ministry of Science and ICT (2019R1A2C1010160), and in part by the Pioneer Research Center Program through NRF of Korea funded by the Ministry of Science and ICT (2014M3C1A3052580). Corresponding author: Han-Youl Ryu (e-mail: hanryu@inha.ac.kr).

**Abstract:** We conducted a systematic investigation of the light extraction efficiency (LEE) of GaN-based vertical micro-scale light-emitting diode ($\mu$-LED) structures using three-dimensional finite-difference time-domain (FDTD) simulations. The LEE of $\mu$-LED structures was found to have a strong dependence on structural parameters such as the shape of the chip cross section, chip dimension, and p-GaN thickness. The LEE of a $\mu$-LED with a circular cross section was lower than that of a $\mu$-LED with a square cross section by 5$\sim$10% owing to the coupling of light with high-quality-factor whispering gallery modes. The LEE of a $\mu$-LED structure decreased as the chip dimension increased, which could be attributed to the increased portion of trapped light inside the LED chip and increased light absorption in the GaN with an increasing chip dimension. In addition, the LEE varied significantly with the thickness of the p-GaN layer, which could be explained by the strong dependence of the angular distribution of the emission pattern on the p-GaN thickness. The FDTD simulation method presented in this study is expected to be advantageously employed in designing $\mu$-LED structures with high LEE.

**Index Terms:** Micro-LED, light-emitting diode, light extraction efficiency, FDTD.

## 1. Introduction

Recently, there has been an increasing interest in micro-scale light-emitting diodes ($\mu$-LEDs), which can be utilized as light sources for deformable displays, optogenetics, and visible light communications [1]–[6]. GaN-based blue $\mu$-LEDs have advantages in such applications in terms of their high luminous efficiency, long lifetime, fast on/off time, and robustness in extreme conditions. As the lateral dimension of $\mu$-LEDs decreases, a higher resolution in displays, higher modulation bandwidth in communications, and lower chip cost are expected to be achieved. To reach a high resolution in displays, $\mu$-LEDs are required with dimensions below 20 $\mu$m. So far, $\mu$-LEDs with dimensions even smaller than 10 $\mu$m have been demonstrated [7]–[11]. Several groups have investigated the effect of the chip dimension on the external quantum efficiency (EQE) of a $\mu$-LED [6], [8]–[13]. It has typically been reported that the EQE of $\mu$-LEDs decreases as the chip dimension

decreases, which has been attributed to increased surface recombination at defects on the side walls of the chip [8], [14], current crowding effects [13], [15], and thermal effects [12].

The EQE is the product of the internal quantum efficiency and the light extraction efficiency (LEE). Because the LEE can also depend on the lateral chip size of a $\mu$-LED, it may have a significant influence on the EQE of a $\mu$-LED. However, the effect of the LEE on the efficiency of $\mu$-LEDs remains relatively unexplored. Because it is difficult to determine the LEE by experimental measurements, the LEE of LEDs has mainly been evaluated by numerical simulations. The finite-difference time-domain (FDTD) method has been widely employed to study the optical characteristics and LEE of GaN-based LED structures where micro- or nano-scale objects are included [15]–[21]. Although accurate simulation results can be obtained using the FDTD method, the computational resources required for FDTD simulations increase considerably as the structure size increases. Therefore, three-dimensional (3-D) FDTD simulations for full-scale LED structures have been challenging.

Nevertheless, the 3-D FDTD method can be employed for the LEE simulation of a vertical chip or thin-film flip-chip structure where the substrate is removed. In this case, the lateral dimension of an LED structure is truncated by imposing metal boundary conditions, assuming that light is mostly emitted through the top surface of the LED chip and the sidewall emission is negligible [16]–[18]. This assumption can be valid because the lateral dimension of a large-area vertical LED chip can be as large as 1 mm whereas the vertical dimension is only several $\mu$ms. Several groups have also presented $\mu$-LED structures with vertical or flip-chip structures for efficient heat dissipation through a small chip area [2], [7], [15], [23]–[25]. However, side-wall emissions cannot be neglected for the simulation of $\mu$-LED structures. The importance role of the side-emission in the angular emission characteristics have been reported in Refs. [26], [27]. Therefore, a full 3-D simulation including the entire $\mu$-LED structure is required to accurately determine the LEE. To our knowledge, few studies have quantitatively evaluated the LEE for $\mu$-LED structures.

In this study, we numerically investigated the LEE for GaN-based vertical $\mu$-LED structures using the 3-D FDTD method. The entire chip structure was included in the computational domain, and the LEE was averaged over the source positions, spectrum, and polarizations, which is expected to yield accurate simulation results for the LEE. Although the reported $\mu$-LED structures have mostly been fabricated with a square cross section, several groups have demonstrated $\mu$-LED structures with a circular cross section [1], [12], [13], [28]. Therefore, we considered $\mu$-LED structures with a square or circular cross section. The LEE was simulated as the lateral chip dimension varied from 5 to 30 $\mu$m, to understand the role of the LEE in the chip-dimension-dependence of the EQE of $\mu$-LEDs. In addition, the dependence of the LEE on the p-GaN thickness was investigated and its dependence was analyzed based on the angular distribution of emission profiles.

## 2. Simulation Structure and Method

For the simulation of this work, a commercial FDTD simulation program by Lumerical Inc. was employed [29]. Fig. 1(a) schematically illustrates the side view of the simulated $\mu$-LED structure in the FDTD computational domain. The entire LED structure was contained inside the computational domain, and the perfectly-matched-layer (PML) boundary conditions were employed on all boundaries of the domain. The layer structures of the $\mu$-LED were composed of a 3-$\mu$m-thick n-GaN layer, 50-nm-thick InGaN/GaN multiple-quantum-well (MQW) active layers, and a p-GaN layer on a high-reflectivity Ag reflector. The refractive index of GaN was set to 2.45, and the InGaN/GaN MQW active region was modeled as a uniform medium with the effective refractive index of 2.49 [30].

The absorption coefficient of the GaN material was varied from 0 to 50 $cm^{-1}$ [31]–[33]. The complex refractive index of Ag was chosen to be $0.14 + 2.47\,i$ [34], which results in a reflectance between the p-GaN and Ag of $\sim$90%. The $\mu$-LED chip was assumed to be enclosed with an epoxy encapsulant with a refractive index of 1.5. In the simulation in this study, we systematically investigated the dependence of the LEE on the chip shape, chip dimension, p-GaN thickness, and the absorption coefficient of GaN.

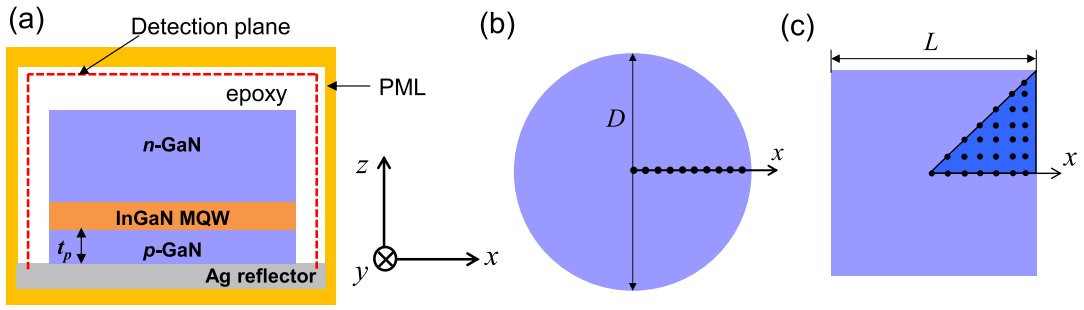


Fig. 1. (a) Schematic side-view ($x$-$z$ plane) diagram of the simulated $\mu$-LED structure. The entire LED structure is contained inside the FDTD computational domain with PML boundaries. (b) and (c) Top-view ($x$-$y$ plane) of the $\mu$-LED structures with circular and square cross sections, respectively. FDTD simulations were performed for each source point, represented as solid dots in (b) and (c). The LEE of $\mu$-LED structures is calculated when varying the thickness of p-GaN [$t_p$ in (a)], diameter of the circular cross section [$D$ in (b)], and side length of the square cross section [$L$ in (c)].

In the FDTD simulation, a single dipole source was placed at the center of the MQW active region in the $z$-direction of Fig. 1(a). The spectral intensity distribution of the dipole source was assumed to follow a Gaussian lineshape function, with a peak wavelength of 450 nm and full-width at half-maximum of 20 nm. For the evaluation of the LEE, the total dipole radiation power was firstly calculated in a small box surrounding the dipole source. Next, the radiation power outside the LED chip was calculated on the detection plane near the PMLs, as indicated by dotted lines in the computational domain in Fig. 1(a). Then, the LEE was determined as the ratio of the power on the detection planes to the total radiated power. The LEE at a position ($x$, $y$) with polarization state $p$ was obtained considering the spectral average of the source spectrum [35].

$$\eta_p(x, y) = \frac{\int \eta_p^{\lambda}(x, y) S(\lambda) d\lambda}{\int S(\lambda) d\lambda}, \tag{1}$$

where $\eta_p^{\lambda}(x, y)$ is the LEE at position ($x$, $y$) and wavelength $\lambda$, and $S(\lambda)$ is the spectral intensity distribution. Here, we considered only $x$ and $y$ directions of the dipole source because InGaN QWs have been known to emit the light polarized mostly in the direction parallel to the QW plane and hence the contribution of the light polarized in the $z$ direction would be negligible [18], [36]–[38]. Because the LEE can depend on the source position and polarization, it is necessary to perform averaging over the active area and two polarization directions in the $xy$ plane. The averaged LEE ($\eta$) can be written as

$$\eta = \frac{\sum_{p=1,2} \int_{area} \eta_p(x, y) dx dy}{2 \int_{area} dx dy}, \tag{2}$$

where $\eta_p(x, y)$ is the LEE at the position ($x$, $y$) with polarization state $p$. For each source position, there are two orthogonal polarization directions: the $x$-polarization and $y$-polarization.

We calculated the LEE for $\mu$-LED structures of circular and square cross section shapes. Fig. 1(b) and (c) shows the cross sectional views of the simulated $\mu$-LEDs in the $xy$ plane for the circular cross section with diameter $D$ and the square cross section with side length $L$, respectively. The solid dots inside each LED structure represent the positions of the dipole sources where the LEE simulation was performed. As shown in Fig. 1(b), for the LED with a circular cross section, it was sufficient to calculate the LEE for the source points in the positive $x$ direction, using its circular symmetry. In this case, $\eta$ for the circular $\mu$-LED with radius $R$ is simplified as [35]

$$\eta = \frac{\sum_{p=1,2} \int_0^R \eta_p(x)(2\pi x) dx}{2\pi R^2} = \frac{1}{R^2} \sum_{p=1,2} \int_0^R \eta_p(x) x dx, \tag{3}$$

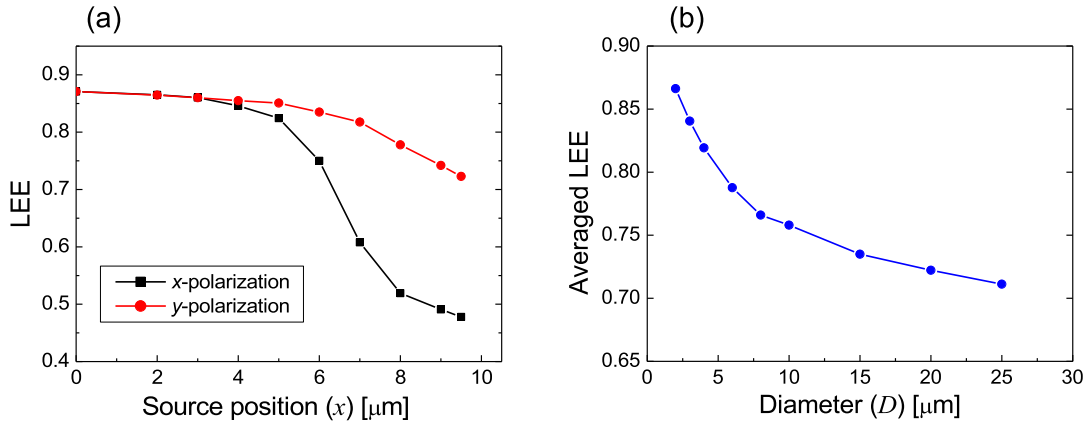


Fig. 2. (a) LEE of the $\mu$-LED with a circular cross section as a function of the source position in the $x$ direction for the $x$- and $y$-polarized dipole sources. Here, the diameter ($D$) is 20 $\mu$m. (b) The LEE averaged over source points and polarizations is plotted as a function of the diameter from 2 to 25 $\mu$m.

where $\eta_p(x)$ is the LEE at position $x$ with polarization state $p$. For example, for the $\mu$-LED with a $D$ value of 20 $\mu$m, 10 source points were used for averaging in Eq. (3), as shown in Fig. 1(b). For the square-shaped LED, it was necessary to consider the source points inside the shaded area in Fig. 1(c) as a result of the square symmetry. For example, with $L$ equal to 20 $\mu$m, the LEE was calculated for 28 source points with two polarization states as shown in Fig. 1(c).

## 3. Results and Discussion

Fig. 2 shows the LEE of the $\mu$-LED with a circular cross section as a function of the source position in the $x$ direction for $D$ equal to 20 $\mu$m. Here, the p-GaN and n-GaN thicknesses were 100 and 3000 nm, respectively. The absorption coefficient of the GaN layers was set to 30 cm$^{-1}$. The highest LEE of $\sim$0.87 was obtained at the center of the LED ($x = 0$), and the LEE maintained high values of $>$0.85 for the source positions with $x < 5$ $\mu$m. However, the LEE begins to decrease rapidly for $x$ greater than 5 $\mu$m, especially for the $x$-polarization. When the source position is near the boundary of the LED, the LEE decreases to below 0.50 for the $x$-polarization. This large decrease in the LEE for the $x$-polarized light is attributed to the coupling of the dipole source with whispering gallery modes (WGMs) that exist along the circumference of the circular boundary [39]. The WGMs generally have high quality factors and polarizations in the radial direction of the circle. Therefore, the $x$-polarized dipole source near the LED boundary can easily couple with the WGMs. The light coupled with the WGM travels along the circumference of the LED and escapes from the LED fairly slowly, resulting in a low LEE.

The averaged LEE was calculated using the data in Fig. 2(a) and Eq. (3). This was obtained as 0.8 for the $y$-polarization and 0.64 for the $x$-polarization. When the LEE was further averaged over the two polarizations, a value of 0.722 was obtained. The LEE of $\mu$-LEDs with a circular cross section was simulated for other diameters between 2 and 25 $\mu$m. Fig. 2(b) shows the average LEE as a function of the diameter ($D$) from 2 to 25 $\mu$m. The averaged LEE gradually decreases as $D$ increases, which can be attributed to the increased light absorption in the GaN layers and Ag reflector with an increasing chip size. The LEE of the circular $\mu$-LED with $D$ between 5 and 25 $\mu$m ranges from 70% to 80%, and it can be increased to $>$85% when $D$ is reduced to $\sim$2 $\mu$m.

Fig. 3 shows the LEE of the $\mu$-LED with a square cross section at the source positions ($x$, $y$) shown in Fig. 1(c) with a side length ($L$) of 20 $\mu$m. The LEE at ($x$, $y$) tends to increase slightly as both $x$ and $y$ increase, and lies between 0.765 and 0.785. However, the difference in the LEE at different source positions is fairly small compared to the case of the circular cross section. Indeed, the largest difference between source points is less than 0.02. The relatively uniform LEE between

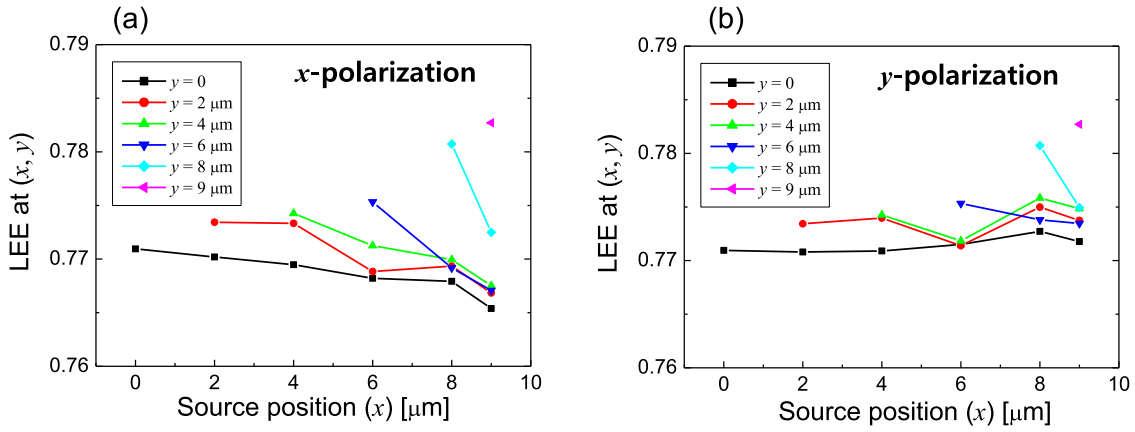


Fig. 3. LEE of the $\mu$-LED with a square cross section at source positions ($x$, $y$) shown in Fig. 1(c) for (a) the $x$ –polarized light and (b) $y$-polarized light. Here, the side length ($L$) is 20 $\mu$m.

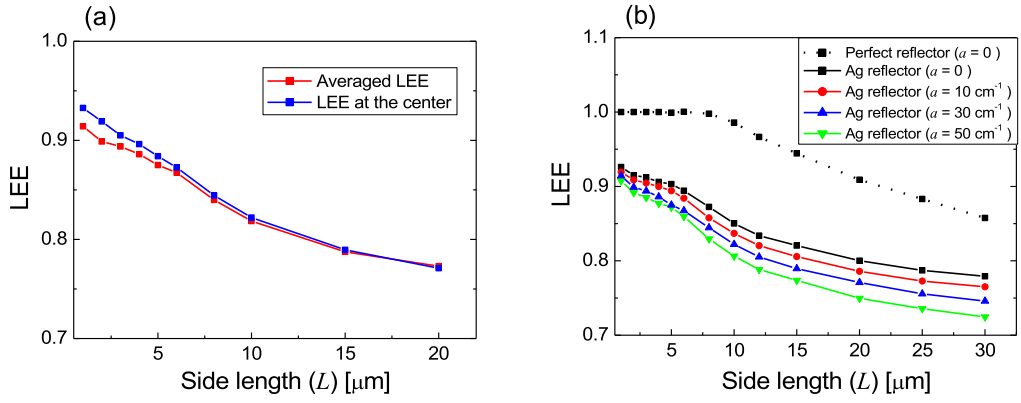


Fig. 4. (a) Averaged LEE and the LEE at the center of the $\mu$-LED with a square cross section as a function of the side length $L$. (b) LEE of the $\mu$-LED with a square cross section as a function of $L$. Solid lines represent the LEE of the $\mu$-LED with the Ag reflector and absorption coefficient of GaN between 0 and 50 cm$^{-1}$. For comparison, the LEE of the $\mu$-LED with the perfect reflector and $a = 0$ is also shown as a dotted line.

source positions implies that the effect of resonant modes such as WGMs is not important in the case of a square cross section. The average and standard deviation of the LEE at ($x$, $y$) are 0.773 and 0.006, respectively. For a precise evaluation of the LEE, it would be necessary to perform averaging over the area and polarization using Eq. (2). However, this averaging process requires too much computational resources. Therefore, we choose the LEE at the origin ($x = y = 0$) as the representative LEE value of $\mu$-LEDs with a square cross section. In this case, the LEE at the origin was 0.771 which deviates from the averaged LEE by only 0.002.

We compared the averaged LEE and the LEE at the center of the $\mu$-LED with a square cross section for other values of the side length from 1 to 15 $\mu$m. Fig. 4(a) shows the averaged LEE and the LEE at the center as a function of $L$. When $L$ is equal to or greater than 10 $\mu$m, the relative difference between the average LEE and the LEE at the center was less than 0.5%. When $L$ is smaller than 10 $\mu$m, the LEE at the center becomes higher than the averaged LEE as $L$ decreases. Therefore, we employ the LEE at the center as the representative LEE value for the square-shaped $\mu$-LED with $L$ equal to or greater than 10 $\mu$m, whereas the averaged LEE is used for the $\mu$-LED with $L$ smaller than 10 $\mu$m.

Fig. 4(b) shows the LEE as a function of $L$ for square-shaped $\mu$-LEDs. Here, the LEE was calculated when the absorption coefficient ($a$) for the p-GaN and n-GaN layers was 0, 10, 30,

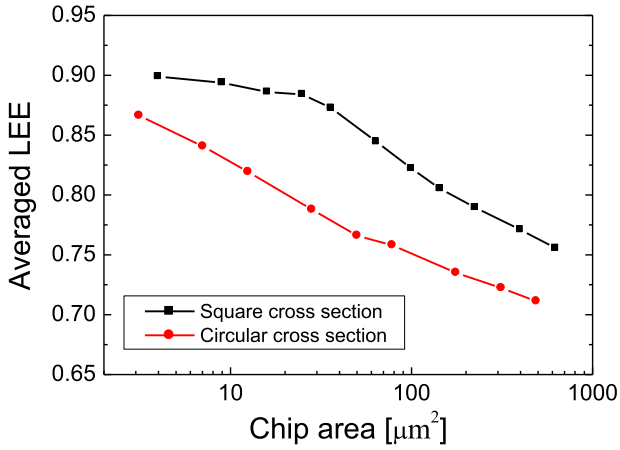


Fig. 5. LEE of $\mu$-LEDs as a function of the cross-sectional area for the square and circular cross sections.

and 50 cm$^{-1}$ for the Ag reflector to observe the effect of optical absorption inside the LED chip. For comparison, the LEE for the perfect reflector with 100% reflectance and $a = 0$ was also simulated to observe the pure geometrical effect excluding any optical loss caused by absorption and reflection. For the case of the perfect reflector without absorption in GaN, the LEE was ~100% when $L$ was less than or equal to 8 $\mu$m. This implies that the escape cone of light inside the LED covers all the surfaces of the square LED chip with $L \leq 8$ $\mu$m. As $L$ increased from 10 to 30 $\mu$m, the LEE decreased from 0.986 to 0.854, implying that the portion of light confined inside the LED chip by the total internal reflection (TIR) increases as the chip size increases. When the perfect reflector was replaced with the Ag reflector, the LEE decreased by 8~12%, which illustrates the importance of the reflectance of the bottom reflector in the LEE. For the case of the Ag reflector, the LEE decreased gradually as $L$ increased, as in the case of the circular cross section in Fig. 2(b). As $a$ increased, the LEE decreased because of the increased light absorption in GaN. When $L = 5$ $\mu$m, the difference between the LEE at $a = 0$ and 50 cm$^{-1}$ was 3.1%. However, this difference increased to 5.5% for $L = 30$ $\mu$m, as a result of the increased influence of light absorption in GaN and Ag with an increasing chip size. The LEE could be higher than 0.8 for $L < 10$ $\mu$m and 0.75 for $L < 20$ $\mu$m unless $a$ was greater than 50 cm$^{-1}$. For $L < 2$ $\mu$m, the LEE can be higher than 0.9. For this small-size chip, the LEE is limited by the light dissipation at the Ag reflector. Note that this relatively high LEE has been achieved without texturing the chip surface.

The LEE is compared for $\mu$-LEDs with circular and square cross sections in Fig. 5. The LEE is plotted as a function of the cross sectional area for the circular and square cross sections. Here, $a$ was fixed at 30 cm$^{-1}$, and the thicknesses of p-GaN and n-GaN were set to 100 and 3000 nm, respectively. For the same chip area, the LEE of the LED with a square cross section was higher than that of the LED with a circular cross section by between 5% and 10%. The lower LEE of the $\mu$-LED with a circular cross section results from the significant decrease in the LEE near the chip boundary owing to the coupling of WGMs as shown in Fig. 2(a). Therefore, the $\mu$-LED with a square cross section is advantageous over that with a circular cross section in terms of achieving a high LEE. So far, we have shown that the LEE of $\mu$-LEDs increases slowly with a decreasing chip dimension. In contrast, the EQE of $\mu$-LEDs has been reported to decrease as the chip dimension decreases, which has been attributed to increased surface recombination and current crowding effects [7], [12]–[14]. If the chip-dimension dependence of the LEE was included, then the effects of surface recombination and current crowding on the EQE could be more significant as the chip dimension decreases.

Next, the dependence of the LEE on the thickness of p-GaN ($t_p$) was investigated for the square-shaped $\mu$-LED. Fig. 6(a) shows the LEE for the total emission, top emission, and side emission

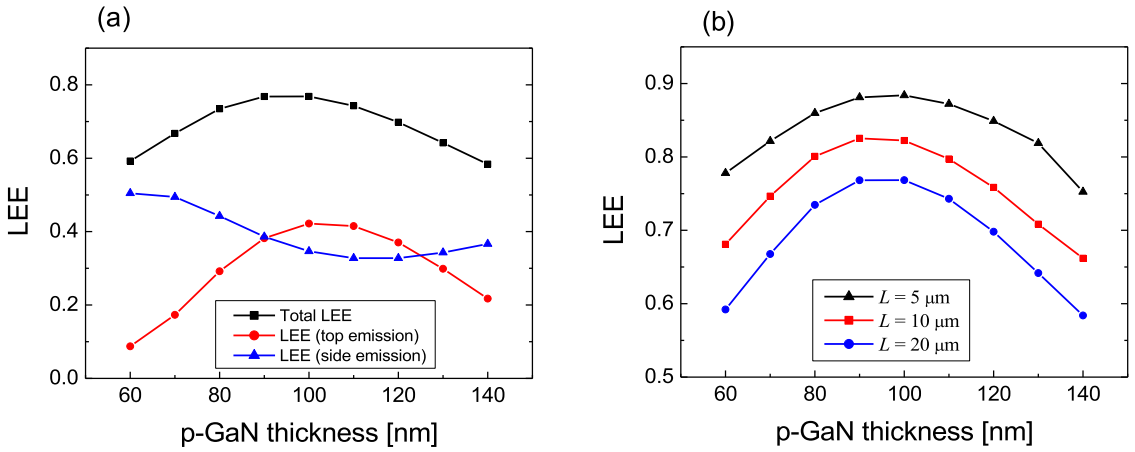


Fig. 6. (a) LEE of the square $\mu$-LED with $L$ equal to 20 $\mu$m as a function of the p-GaN thickness ($t_p$). The LEE for the top and side emissions is shown separately. The total LEE is the sum of the top-emission and side-emission LEEs. (b) Total LEE as a function of the p-GaN thickness for $L$ of 5, 10, and 20 $\mu$m.

as a function of $t_p$ between 60 and 140 nm with $L$ equal to 20 $\mu$m. The LEE is observed to be strongly dependent on the p-GaN thickness. The highest total LEE of ~0.77 was obtained at $t_p$ equal to 90 and 100 nm. The total LEE decreases as $t_p$ decreases below 80 nm or increases over 110 nm. Indeed, it decreases to below 0.6 when $t_p$ is 60 or 140 nm. The top-emission LEE exhibits the same dependence on the p-GaN thickness as the total LEE, whereas the side-emission LEE has a dependence opposite to the total or top-emission LEE. The large variations in the top- and side-emission LEE values with $t_p$ implies that the LEE can be related to the emission profile, which is strongly influenced by the thickness of the p-GaN layer. Because the interference pattern of the light emitted from the QWs with the light reflected at the Ag reflector depends on the relative distance between the QWs and Ag, the emission profile, and hence the LEE, can be dependent on $t_p$. This light interference effect in vertical or flip-chip structures has also been reported in previous works [16]–[18], [40]. The dependence of the LEE on $t_p$ was also investigated for other $L$ values. Fig. 6(b) compares the total LEE as a function of $t_p$ for $L$ of 5, 10, and 20 $\mu$m. The variation of the LEE shows a similar trend with the variation of $t_p$. That is, the maximum value of the LEE was obtained around $t_p$ of 100 nm for all $L$ values from 5 to 20 $\mu$m. For a given p-GaN thickness, the LEE increased as $L$ decreased,

To understand the effect of $t_p$, the angular distribution of the emission profile was calculated. Fig. 7 shows the two-dimensional polar plot of the electric field intensity profile for $t_p$ equal to 60, 80, 90, 100, 120, and 140 nm. For this simulation, the absorption coefficient of the GaN layers was set to 30 $cm^{-1}$. The angular distribution is observed to vary considerably with the p-GaN thickness. For $t_p$ equal to 60 nm, a strong side emission is observed, resulting in a high side-emission LEE and low top-emission LEE, as shown in Fig. 6. In contrast, for $t_p$ between 80 and 100 nm, a relatively strong emission in the vertical direction is observed, resulting in a low side-emission LEE and high top-emission LEE. For $t_p$ of 120 and 140 nm, a relatively high intensity is observed in the polar angle between 30° and 50°.

In the simulated $\mu$-LED structure, the critical angle of TIR is calculated as $\sin^{-1}(1.5/2.5)$ ~37°. Therefore, the light incident on the top surface with an angle larger than 37° may undergo TIR. However, the light with an incident angle greater than 53° can escape through the side-walls of the $\mu$-LED when it is incident on the side-wall surface after reflecting at the top surface. Consequently, the light with incidence angle between 37° and 53° can be trapped inside the LED structure. For $t_p$ of 140 nm, a high intensity was observed within this angular range, resulting in a low LEE, as shown in Fig. 6. The side-emitting light in Fig. 7(a) can mostly escape through the side-wall of the $\mu$-LED structure without TIR. However, the side-emitting light undergoes increased light absorption

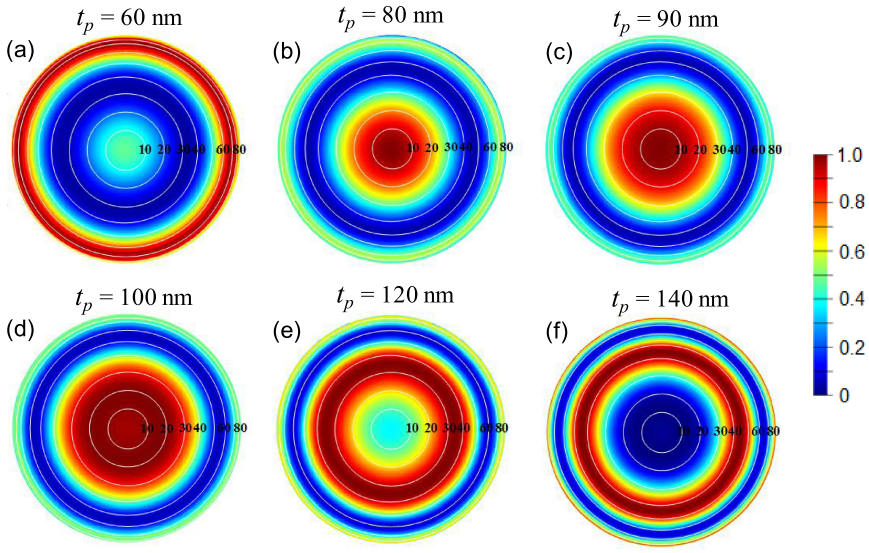


Fig. 7. Two-dimensional polar plot of the angular distribution of emission patterns for p-GaN thicknesses ($t_p$) of (a) 60, (b) 80, (c) 90, (d) 100, (e) 120, and (f) 140 nm. The polar angles from 0 to 80° are indicated on each figure. A color-scale bar is shown at the right side of the figure, where the highest intensity is normalized to 1.

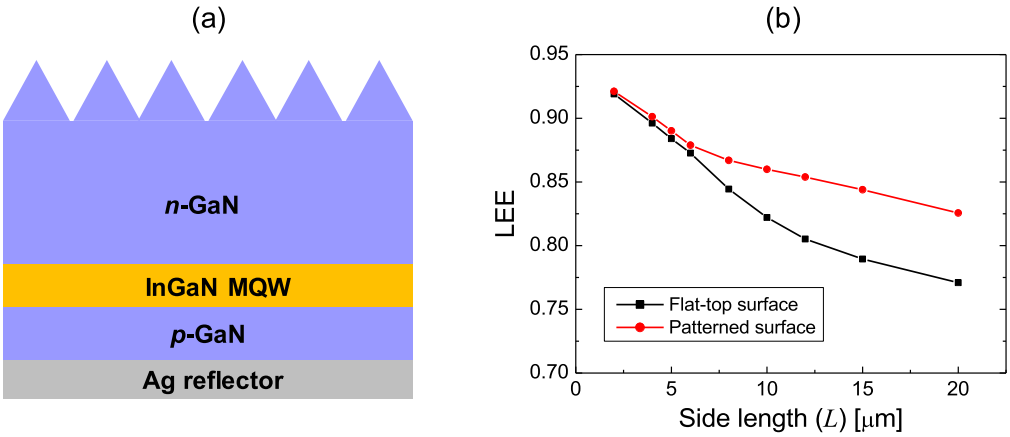


Fig. 8. Two-dimensional polar plot of the angular distribution of emission patterns for p-GaN thicknesses ($t_p$) of (a) 60, (b) 80, (c) 90, (d) 100, (e) 120, and (f) 140 nm. The polar angles from 0 to 80° are indicated on each figure. A color-scale bar is shown at the right side of the figure, where the highest intensity is normalized to 1.

when it traverses the LED structure compared with the case of the top-emitting light because the chip length (20 $\mu$m) is significantly longer than the chip thickness ($\sim$3.1 $\mu$m). That is, the low LEE for $t_p$ of 60 nm can be attributed to the large absorption loss in the GaN layers. The result of Fig. 7 implies that a high LEE can be obtained by adopting a suitable p-GaN thickness to achieve an optimum emission profile.

Finally, the effect of surface patterning on the LEE of $\mu$-LED structures was investigated. Fig. 8(a) shows a schematic side-view diagram of a $\mu$-LED structure with patterns on the n-GaN surface. The patterns were assumed to be a two-dimensional array of GaN cones. Fig. 8(b) compares the LEE of $\mu$-LED structures with flat-top and patterned surfaces as the side length $L$ varied. Here, the absorption coefficient of the GaN layers was again set to 30 cm$^{-1}$. In Fig. 8(b), the bottom

diameter, height, and period of cone patterns were all assumed to be 1 $\mu$m. However, we found that similar results on the LEE were obtained for other dimensions of the cone patterns. When *L* was larger than 6 $\mu$m, the LEE of the patterned surface was higher than that of the flat-top surface. This is because the portion of light trapped by TIR increases with increasing chip dimension for the structure with flat-top surface, whereas the TIR can be spoiled by cone patterns for the structure with patterned surface. However, for *L* equal to or greater than 6 $\mu$m, the difference in the LEE between the two structures was negligible, implying all surfaces are within the escape cone of emitted light for the structure with flat-top surface. For this small chip dimension, a high LEE $>$85% could be obtained without surface patterning.

## 4. Conclusion

In summary, the structural parameter dependence of the LEE of GaN-based vertical-chip $\mu$-LED structures was systematically investigated using 3-D FDTD simulations. To obtain accurate simulation results for the LEE, we performed a full-structure simulation with averaging over the spectral distribution, dipole source positions, and source polarizations. The LEE of the $\mu$-LED with a circular cross section was found to be 5$\sim$10% lower than that of the $\mu$LED with a square cross section for the same chip area, resulting from the coupling of high-quality-factor WGMs in the circular-shaped LED. A decrease in the LEE with an increasing chip dimension was also observed. This is because the portion of light trapped inside the LED chip and the absorption in the GaN layers and Ag reflector increased as the chip dimension increased. In addition, the thickness of the p-GaN layer was found to have a strong influence on the LEE. This can be explained by the angular distribution of the emission pattern, which varies significantly with the p-GaN thickness owing to the interference of light reflected at the Ag reflector. A high LEE could be obtained at a p-GaN thickness where the vertical emission was dominant. These strong dependences of the LEE on certain structural parameters should be considered when analyzing the EQE for $\mu$-LED structures. The FDTD simulation results of this study are expected to provide insights into the optical characteristics of $\mu$-LED structures, and hence the design of high-efficiency $\mu$-LEDs.

## References


[1] H. X. Jiang, S. X. Jin, J. Li, J. Shakya, and J. Y. Lin, "III-nitride blue microdisplays," *Appl. Phys. Lett.*, vol. 78, no. 9, pp. 1303–1305, 2001.

[2] Z. J. Liu, K. M. Wong, C. W. Keung, C. W. Tang, and K. M. Lau, "Monolithic LED microdisplay on active matrix substrate using flipchip technology," *IEEE J. Sel. Topics Quantum Electron.*, vol. 15, no. 4, pp. 1298–1302, Jul./Aug. 2009.

[3] S. W. H. Chen *et al.*, "Full-color monolithic hybrid quantum dot nanoring micro light-emitting diodes with improved efficiency using atomic layer deposition and nonradiative resonant energy transfer," *Photon. Res.*, vol. 7, no. 4, pp. 416–422, 2019.

[4] F. Wu, E. Stark, P. C. Ku, K. D. Wise, G. Buzsaki, and E. Yoon, "Monolithically integrated LEDs on silicon neural probes for high-resolution optogenetic studies in behaving animals," *Neuron*, vol. 88, no. 6, pp. 1136–1148, 2015.

[5] S. Rajbhandari *et al.*, "A review of gallium nitride LEDs for multi-gigabit-per-second visible light data communications," *Semicond. Sci. Technol.*, vol. 32, no. 2, 2017, Art. no. 023001.

[6] Y. Huang, G. Tan, F. Gou, M. C. Li, S. L. Lee, and T. S. Wu, "Prospects and challenges of mini-LED and micro-LED displays," *J. Soc. Inf. Display*, vol. 27, pp. 387–401, 2019.

[7] C. J. Chen, H. C. Chen, J. H. Liao, C. J. Yu, and M. C. Wu, "Fabrication and characterization of active-matrix 960 $\times$ 540 blue GaN-based micro-LED display," *IEEE J. Quantum Electron.*, vol. 55, no. 2, Apr. 2019, Art. no. 3300106.

[8] P. Tian *et al.*, "Side-dependent efficiency and efficiency droop of blue InGaN micro-light emitting diodes," *Appl. Phys. Lett.*, vol. 101, no. 23, 2012, Art. no. 231110.

[9] F. Olivier, S. Tirano, L. Dupré, B. Aventurier, C. Largeron, and F. Templier, "Influence of size-reduction on the performances of GaN-based micro-LEDs for display application," *J. Lumin.*, vol. 191, pp. 112–116, 2017.

[10] D. Hwang, A. Mughal, C. D. Pynn, S. Nakamura, and S. DenBaars, "Sustained high external quantum efficiency in ultrasmall blue III-nitride micro-LEDs," *Appl. Phys. Exp.*, vol. 10, no. 3, 2017, Art. no. 032101.

[11] D. Hwang *et al.*, "Micro-light-emitting diodes with III-nitride tunnel junction contacts grown by metalorganic chemical vapor deposition," *Appl. Phys. Exp.*, vol. 11, no. 1, 2018, Art. no. 012102.

[12] H. Huang, H. Wu, C. Huang, Q. Han, C. Wang, and H. Wang, "Thermal effects on the electrical and optical characteristics of micro-light-emitting diodes with different current spreading layer," *Phys. Status Solidi A*, vol. 216, no. 14, 2019, Art. no. 1900006.

[13] C. C. Li *et al.*, "Operating behavior of micro-LEDs on a GaN substrate at ultrahigh injection current densities," *Opt. Exp.*, vol. 27, no. 16, pp. A1146–A1155, 2019.

[14] M. S. Wong *et al.*, "High efficiency of III-nitride micro-light-emitting diodes by sidewall passivation using atomic layer deposition," *Opt. Exp.*, vol. 26, no. 16, pp. 21324–21331, 2018.
[15] W. Guo *et al.*, "Origins of inhomogeneous light emission from GaN-based flip-chip green micro-LEDs," *IEEE Electron Device Lett.*, vol. 40, no. 7, pp. 1132–1135, Jul. 2019.
[16] D. Wu, P. Ma, B. Liu, S. Zhang, J. Wang, and J. Li, "Improved light extraction efficiency of GaN-based flip-chip light-emitting diodes with an antireflective interface layer," *AIP Adv.*, vol. 6, no. 5, 2016, Art. no. 055201.
[17] H. Y. Ryu and J. I. Shim, "Structural parameter dependence of light extraction efficiency in photonic crystal InGaN vertical light-emitting diode structures," *IEEE J. Quantum Electron.*, vol. 46, no. 5, pp. 714–720, May 2010.
[18] P. Zhao and H. Zhao, "Analysis of light extraction efficiency enhancement for thin-film-flip-chip InGaN quantum wells light-emitting diodes with GaN micro-domes," *Opt. Exp.*, vol. 20, no. S5, pp. A765–A776, 2012.
[19] H. Y. Ryu, "Modification of internal quantum efficiency and efficiency droop in GaN-based flip-chip light-emitting diodes via the purcell effect," *Opt. Exp.*, vol. 23, no. 19, pp. A1157–A1166, 2015.
[20] P. Zhu and N. Tansu, "Effect of packing density and packing geometry on light extraction of III-nitride light-emitting diodes with microsphere arrays," *Photon. Res.*, vol. 3, no. 4, pp. 184–191, 2015.
[21] P. Du and Z. Cheng, "Enhancing light extraction efficiency of vertical emission of AlGaN nanowire light emitting diodes with photonics crystal," *IEEE Photon. J.*, vol. 11, no. 3, Jun. 2019, Art. no. 1600109.
[22] D. Han *et al.*, "Enhanced light extraction efficiency of a InGaN/GaN micro-square array light-emitting diode chip," *Opt. Mat. Exp.*, vol. 7, no. 9, pp. 3261–3269, 2017.
[23] P. Tian *et al.*, "Fabrication, characterization, and applications of flexible vertical InGaN micro-light emitting diode arrays," *Opt. Exp.*, vol. 24, no. 1, pp. 699–707, 2016.
[24] Z. Zhou, B. Yan, X. Ma, D. Teng, L. Liu, and G. Wang, "GaN-based mid-power flip-chip light-emitting diode with high -3 dB bandwidth for visible light communications," *Appl. Opt.*, vol. 57, no. 11, pp. 2773–2779, 2018.
[25] F. B. Chne, K. L. Chi, W. Y. Yen, J. K. Sheu, M. L. Lee, and J. W. Shi, "Investigation on modulation speed of photon-recycling white light-emitting diodes with vertical-conduction structure," *J. Lightw. Technol.*, vol. 37, no. 4, pp. 1225–1230, Feb. 2019.
[26] K. Kang, J. Yoon, J. Kim, H. Lee, and B. Yang, "Effect of the finite pixel boundary on the angular emission characteristics of top-emitting organic light-emitting diodes" *Opt. Exp.*, vol. 23, no. 11, pp. A709–A717, 2015.
[27] F. Gou *et al.*, "Angular color shift of micro-LED displays," *Opt. Exp.*, vol. 27, no. 12, pp. A746–A757, 2019.
[28] P. Tian *et al.*, "Characteristics and applications of micro-pixelated GaN-based light emitting diodes on Si substrates," *J. Appl. Phys.*, vol. 115, no. 3, 2014, Art. no. 033112.
[29] *FDTD*. Vancouver, BC, Canada: Lumerical Inc., 2019. [Online]. Available: http://www.lumerical.com/products/fdtd/
[30] G. M. Laws, E. C. Larkins, I. Harrison, C. Molloy, and D. Somerford, "Improved refractive index formulas for the $Al_xGa_{1-x}N$ and $In_yGa_{1-y}N$ alloys," *J. Appl. Phys.*, vol. 89, no. 2, pp. 1108–1115, 2001.
[31] O. Ambacher, W. Rieger, P. Ansmann, H. Angerer, T. D. Moustakas, and M. Stutzmann, "Sub-bandgap absorption of gallium nitride determined by photothermal deflection spectroscopy," *Solid State Commun.*, vol. 97, no. 5, pp. 365–370, 1996.
[32] H. Y. Ryu, K. S. Jeon, M. G. Kang, Y. Choi, and J. S. Lee, "Dependence of efficiencies in GaN-based vertical blue light-emitting diodes on the thickness and doping concentration of the n-GaN layer," *Opt. Exp.*, vol. 21, no. S1, pp. A190–A200, 2013.
[33] J. Sung *et al.*, "Effect of light absorption in InGaN/GaN vertical light-emitting diodes," *J. Nanoscience Nanotechnol.*, vol. 15, no. 7, pp. 5135–5139, 2015.
[34] E. D. Palik, *Handbook of Optical Constants of Solids*. Cambridge, MA, USA: Academic Press, 1998.
[35] H. Y. Ryu, "Evaluation of light extraction efficiency of GaN-based nanorod light-emitting diodes by averaging over source positions and polarizations," *Crystals*, vol. 8, 2018, Art. no. 27.
[36] S. L. Chuang, "Optical gain of strained wurtzite GaN quantum-well lasers," *IEEE J. Quantum Electron.*, vol. 32, no. 10, pp. 1791–1800, Oct. 1996.
[37] H. Zhao, R. A. Arif, Y. K. Ee, and N. Tansu, "Self-consistent analysis of strain-compensated InGaN-AlGaN quantum wells for lasers and light-emitting diodes," *IEEE J. Quantum Electron.*, vol. 45, no. 1, pp. 66–78, Jan. 2009.
[38] T. Kolbe *et al.*, "Optical polarization characteristics of ultraviolet (In)(Al)GaN multiple quantum well light emitting diodes," *Appl. Phys. Lett.*, vol. 97, no. 17, 2010, Art. no. 171105.
[39] S. L. McCall, A. F. J. Levi, R. E. Slusher, S. J. Pearton, and R. A. Logan, "Whispering-gallery mode microdisk lasers," *Appl. Phys. Lett.*, vol. 60, pp. 289–291, 1992.
[40] Y. C. Shen *et al.*, "Optical cavity effects in InGaN/GaN quantum-well-heterostructure flip-chip light-emitting diodes," *Appl. Phys. Lett.*, vol. 82, no. 14, pp. 2221–2223, 2003.